Nanoscale

PAPER

View Article Online
View Journal | View Issue

Cite this: *Nanoscale*, 2018, **10**, 9899

The size-selective interaction of key and lock nanocrystals driven by depletion attraction at the nanoscale†

D. Hinrichs, R. Himstedt and D. Dorfs *

In this article, we study the size-dependent interactions of quasi-spherical nanocrystals with voids of concave nanoparticles of complementary sizes and shapes. Experimental insights into a system with key and lock particles with smaller dimensions than 15 nm are presented, which provide evidence for key–lock specific interaction on this length scale. Using depletion attraction as a driving force, the key–lock interaction is shown to be reversible and independent of the material composition of the key particles. Poly(ethylene glycol) methacrylate was utilized as a depletion agent in toluene, the solvent of the studied key–lock system. For this work, a model system of specifically developed concave manganese oxide nanocrystals, synthesized *via* a cast–mold approach, in combination with highly monodisperse quasi-spherical gold nanocrystals, was investigated with transmission electron microscopy, optical UV/vis/NIR spectroscopy and powder X-ray diffraction. Size-dependent key–lock interactions are clearly identified to occur. For geometrical reasons, only key particles with smaller particle diameters than the voids of the complementary lock particles are able to enter the void. So the void diameter of the lock particles sets a diameter threshold for the key–lock interaction. Additionally, other key particles like silver, iron oxide and even core–shell structured gold-nickel sulfide nanocrystals show key-in-lock assemblies with concave manganese oxide nanocrystals. This behaviour might open up new routes for size-selective particle sensing.

Received 6th March 2018,
Accepted 28th March 2018

DOI: 10.1039/c8nr01893f

rsc.li/nanoscale

Introduction

Despite many examples of specific interactions of colloidal particles containing cavities at the mesoscale, such systems with particles at the nanoscale are rarely studied.[1,2] This is because the preparation of nanoparticles with specific concave-shaped particle domains is still challenging. Additionally, the commonly used optical microscopy for the analysis of the particle–particle interactions is not applicable at this small dimension any more.

Due to these complications, the investigations of feasible key–lock systems at the nanoscale were done mostly theoretically.[3–7]

Only two experimental studies at the nanoscale have been published so far. George and co-workers prepared concave iron oxide nanoparticles by a cast–mold approach in 2011.[1] Mixing these lock particles with complementary gold nanocrystals resulted in the destabilization of the gold colloid. They concluded, based on their data, that some kind of key–lock interaction had taken place. Thereby ligands could be stripped from the gold nanocrystal surface, presumably resulting in particle destabilization. Furthermore, in 2014, Kraus-Ophir and co-workers prepared a polymer film on a conducting tin-doped indium oxide support, with nanometre-sized cavities by nanoparticle-imprinting and subsequent dissolution of these particles.[2] Using this macroscopic specimen, they could indirectly analyse the amount of gold nanoparticles taken up by the voids by measuring the charge, which was needed for the complete electro-oxidation. Both experimental studies were conducted only with gold as the material for the "key" particles, and the procedure in both cases inherently destroyed the investigated gold nanocrystals.

In general, at the mesoscale, lock particles are prepared *via* 2D and 3D lithography,[8–11] controlled shell buckling of polymerized silicon oil droplets without templates,[12,13] or growth on template particles.[14,15] Beside various possible interparticle forces, *e.g.* van der Waals, magnetic, electrostatic and molecular, mostly the entropic effect of depletion interaction was used as the driving force to initiate the key–lock self-assem-

Department of Physical Chemistry and Electrochemistry, Leibniz Universität Hannover, Callinstrasse 3A, 30167 Hannover, Germany. E-mail: dirk.dorfs@pci.uni-hannover.de

†Electronic supplementary information (ESI) available: Additional UV/vis/NIR extinction spectra, TEM overview images, data of the cyanide etching, size and the phase determination of key particles. See DOI: 10.1039/c8nr01893f

bly.[16] Although theoretical studies predict the key–lock interactions initiated *via* depletion interaction at the nanoscale, this driving force was never used experimentally for such a system so far.[3,4,7]

In this paper, we show an experimental study of a novel key–lock system at the nanoscale. We design tailored lock particles consisting of concave-shaped manganese oxide nanocrystals prepared *via* a cast–mold approach. In addition, highly monodisperse key nanocrystals consisting of various materials are synthesised, *e.g.* gold, silver, iron oxide and gold-nickel sulfide hybrid nanocrystals. Utilizing depletion attraction as the entropic driving force, the key-in-lock assemblies of these highly crystalline nanoparticles are analysed by transmission electron microscopy. We demonstrate their size-specific but simultaneously material-independent interaction. Furthermore, the assembly is shown to be reversible *via* dilution of the colloidal solution.

The gathered results of the size-selective nanoparticle interaction are essential for prospective applications, *e.g.* an analytically used nanoparticle colloid with size-selective nanoparticle recognition properties.

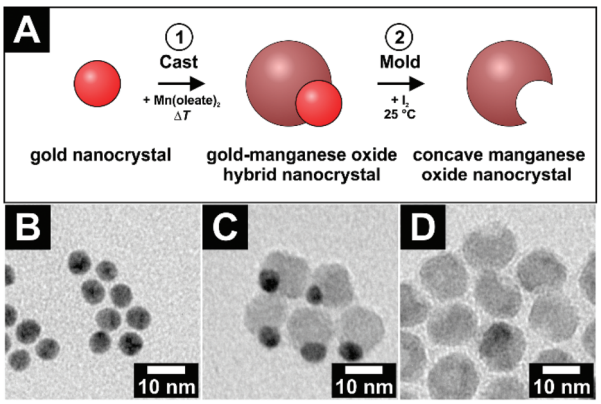

Fig. 1 (A) Panel A shows a scheme of the cast–mold approach, which is used to obtain concave manganese oxide nanocrystals. In the first step, manganese oxide is grown onto quasi-spherical gold nanocrystals *via* the thermal decomposition of manganese oleate. In the second step, the gold domain of the hybrid nanocrystals is etched by iodine. Thereby a void complementary to the shape and size of the gold nanocrystal is formed inside the manganese oxide nanocrystals. (B–D) TEM bright field images of (B) gold nanocrystals with diameters of (6.4 ± 0.5) nm, (C) gold-manganese oxide hybrid nanocrystals with an outer diameter of (12.7 ± 1.3) nm, and (D) the respective etched particles with a spheroidal void with an aperture of around (5.5 ± 0.7) nm.

Results and discussion

Concave manganese oxide nanocrystals

Concave nanocrystals or, that means nanoparticles with an accessible void, were synthesized *via* the so-called cast–mold-approach.[1] In general, this procedure consists of two steps: first, a material is grown onto a template of a different material, which has a specific size and shape. Afterwards, this template is removed *via* an etching process. A void is obtained in the on-grown material with the size and shape of the template. In this work, manganese oxide nanocrystals (MONCs) with concave-shaped regions not yet reported were produced *via* the nucleation and growth of manganese oxide onto preformed quasi-spherical gold nanocrystals (AuNCs) with a highly monodisperse size distribution. The gold domain of these asymmetric hybrid nanocrystals was removed by etching with iodine afterwards. The etching can only be achieved if the gold domain is in contact with the nanoparticle surface. Only in this case iodine is able to reach and etch the gold. Iodine cannot etch the manganese oxide domain itself. Therefore, the manganese oxide domain stays unchanged in size and shape. Thereby, highly crystalline MONCs, each containing a spheroidal void, could be obtained (for details, see the Experimental section). It should be noted here that manganese oxide was chosen as the material simply and only due to the relatively simple and highly reproducible synthesis procedure for the concave MONCs and not because of any type of specific chemical interaction of this material. Thus, in principle, similar key–lock recognition should be possible with any type of colloidal particles, which can be prepared sufficiently monodisperse with similar spheroidal voids. In Fig. 1A, the schematic reaction pathway is drawn. Starting from AuNCs with an initial diameter of (6.4 ± 0.5) nm (Fig. 1B), an exemplary system of hybrid Au–MONCs was grown with an outer diameter of (12.7 ± 1.3) nm (Fig. 1C). The gold domains were removed to obtain concave MONCs with a spheroidal void (Fig. 1D). With (5.5 ± 0.7) nm, the aperture of these voids is slightly smaller than the pristine AuNC diameter. This difference of 1 nm is a result of the hybrid nanocrystal geometry. The gold nanocrystal is less than half overgrown by the manganese oxide. Therefore, the imprint in the manganese oxide is smaller than the diameter of the gold.

The exact geometry of the Au–MONC hybrid particles can be tuned by varying the number of manganese oxide nucleation sides per gold particle. To obtain asymmetric Janus-like hybrid particles with one manganese oxide domain per particle, a preliminary ligand exchange for the AuNCs from oleylamine to octadecanethiol is necessary.[17] The much higher binding affinity of the thiol group to gold in comparison with an amine group suppresses multiple nucleations of manganese oxide on the thiol-protected surface of one gold particle. So, only one manganese oxide domain per AuNC will nucleate and Janus-like hybrids will be obtained. Without such a ligand exchange, multiple nucleations of manganese oxide per AuNC initiate the growth of flower-like hybrid particles.

Interestingly, multiple nucleations of manganese oxide on large gold nanocrystals open up the possibility of creating large voids, which are formed by up to four fused manganese oxide domains (see Fig. S1 and S2†). Most frequently, particles with two or three fused domains can be found. In Fig. 2A and B such Au–MONCs and concave MONCs with an outer diameter of roughly 25 nm to 30 nm and an inner void diameter of (9.3 ± 0.9) nm are shown. Because approximately half of each AuNC is overgrown with manganese oxide, the aperture

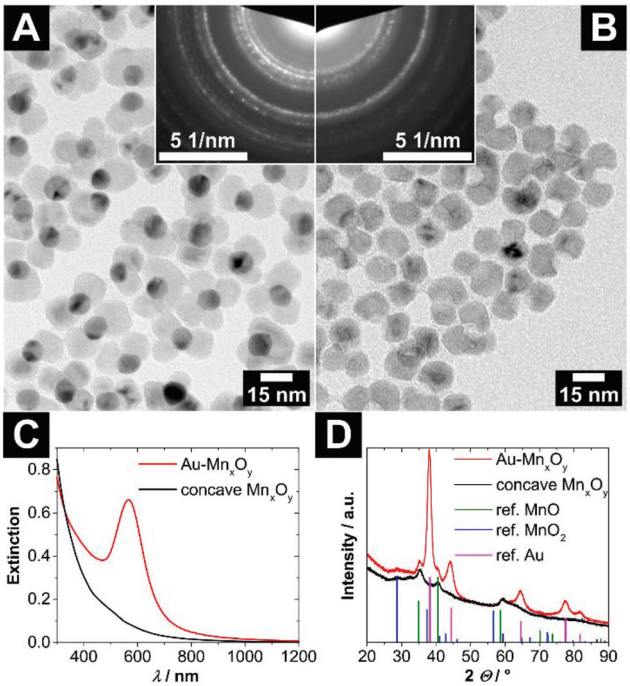

Fig. 2 (A) TEM bright field image of hybrid Au–MONCs with a (10.8 ± 0.8) nm large gold domain. The upper right inlay shows the selected area electron diffraction of these hybrid nanocrystals. (B) TEM bright field image of the same particles after etching of the gold domains *via* iodine. In the upper left inlay, the selected area electron diffraction of these concave MONCs is depicted. The assignment of the ring patterns is given in Fig. S4 (ESI†). (C) UV/vis/NIR extinction spectra of the Au–MONCs and concave MONCs. (D) Powder X-ray diffraction patterns of the Au–MONCs and the respective concave MONCs. The reference structural data show the reflection positions of manganosite (MnO, PDF card #: 01-075-6876), pyrolusite (MnO_2, PDF card #: 01-071-0071), and gold (Au, PDF card #: 00-004-0784) displayed as vertical lines.

of the voids has nearly the same diameter as the inner void in this case.

The UV/vis/NIR extinction spectrum of the hybrid Au–MONCs in Fig. 2C shows an absorption band at around 566 nm, which originates from the localized surface plasmon resonance (LSPR) of the gold domain. In comparison with the position of the resonance frequency of the pristine AuNCs, which is located at 531 nm (see Fig. S3†), the LSPR band of the hybrid Au–MONCs is shifted bathochromically. The reason for this is the higher dielectric permittivity of manganese oxide in contrast to toluene. After the treatment of the hybrid Au–MONCs with iodine to dissolve the gold domains, the concave MONCs show a non-characteristic absorption, which increases towards shorter wavelengths. No LSPR-induced absorption can be found any more. This is a strong indicator for the complete absence of all gold domains within the whole sample.

The powder XRD patterns in Fig. 2D are in line with the optical measurements. The reflections of gold in the hybrid Au–MONCs at 38.2, 44.4, 64.6, 77.5 and 81.7° 2Θ disappear after iodine treatment. Furthermore, also in the TEM investigation (Fig. 2B), no gold can be found after iodine treatment. All in all, these findings prove the quantitative absence of gold after the etching procedure. However, the powder XRD patterns show that the manganese oxide domains of the hybrid nanocrystals as well as of the concave nanocrystals are not a pure phase, but rather a mixture of mainly manganosite and pyrolusite.

The synthesis of concave manganese oxide nanocrystals *via* the described cast–mold approach is highly versatile. Using AuNCs with different diameters makes it possible to obtain concave nanocrystals with differently sized void apertures; see the ESI for details (Fig. S5†).

Besides gold etching with iodine, which yields well-shaped and quantitative gold-free concave MONCs, there is also the possibility of using cyanide to dissolve all gold domains. The iodine procedure has one drawback: already small amounts of residual iodine on the surface of the concave MONCs can interfere with the consecutive key–lock experiments by inducing AuNC coalescence (see the section 'Key and lock interaction'). Therefore, it is essential to thoroughly clean the etched product. However, etching the gold *via* a two-phase reaction using an aqueous potassium cyanide solution also yields concave MONCs. To obtain a colloidal stable and quantitatively gold-free product, the addition of a phase-transfer catalyst is necessary (here: 18-crown-6-ether). This fact is inherently connected to a drawback of this method. The cyanide ions in the organic phase are so strongly activated[18,19] that they do not only etch the gold domains but also significantly dissolve parts of the manganese oxide phase. Especially the inner region is affected, which was the pristine surrounding of the seed (see Fig. S6† for details). Interestingly, the broadening of the void diameters can be used as some kind of post-synthetic fine-tuning for the void diameters of a given Au–MONC batch. All in all, the iodine-based etching procedure in combination with a thorough cleaning of the product results in more defined voids than those from the cyanide procedure.

Independent of the type of etching procedure used, whether iodine or potassium cyanide in combination with 18-crown-6-ether, we would like to emphasise that it is extremely important to thoroughly check the concave product whether the etching procedure was quantitative for all particles (*e.g.* TEM, UV/vis, SAED). Otherwise the remaining gold could lead to misinterpretation of the later key–lock experiments.

Quasi-spherical gold nanocrystals

For the investigation of size-specific interparticle interactions of concave and convex nanocrystals, not only monodisperse voids are necessary. Also, highly monodisperse convex particles with an almost spherical shape are needed, to keep the system as simple as possible and to gain information about the interaction of the specific combination of just one particle size with a specific void size. Therefore, gold nanocrystals provided the best opportunities for this purpose, due to their well-developed synthesis procedure.

Quasi-spherical gold nanocrystals (AuNCs), which are soluble in organic solvents, could be synthesized in various diameters with very narrow size distributions by varying the

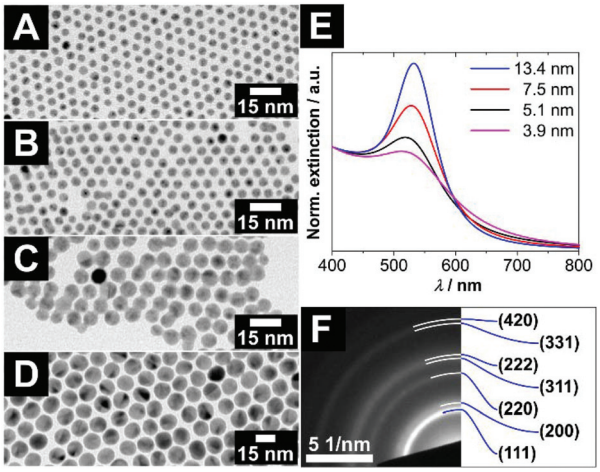

Fig. 3 (A–D) TEM bright field images of highly monodisperse, oleylamine stabilized, quasi-spherical gold nanocrystals with various diameters of (A) (3.9 ± 0.3) nm, (B) (5.1 ± 0.6) nm, (C) (7.5 ± 0.6) nm and (D) (13.4 ± 0.9) nm. Additional overview images and size distributions can be found in Fig. S7 (ESI†). (E) Normalised UV/vis extinction spectra of the differently sized gold nanocrystals. (F) The panel shows a selected area electron diffraction of ≈5 nm large gold nanocrystals with assigned lattice planes of *fcc* gold.

reaction temperature and utilising a seed-mediated growth approach. The diameters of the AuNCs increase with decreasing reaction temperature. AuNCs with larger diameters than approx. 6–7 nm can only be obtained *via* seed-mediated growth. For details, see the Experimental section. In Fig. 3A–D, a selection of AuNCs is depicted, which were used for further investigation of the key and lock interaction later on. The UV/vis extinction spectra of these AuNCs in Fig. 3E show absorption bands between 500 nm and 600 nm, which are typical for gold nanoparticles. The origin of these absorption bands is the localized surface plasmon resonance (LSPR) of the conduction band electrons of the gold. In the short-wavelength regime at and below 400 nm, the absorption is mostly caused by interband transitions. Thereby it is proportional to the gold mass concentration and independent of the nanocrystal size.[20] Hence, the spectra were normalised at 400 nm for a better comparability of the LSPR-induced absorption bands. In general, three tendencies can be gathered comparing the normalised UV/vis extinction spectra of the gold nanocrystals, which are expected for monodisperse gold nanocrystals. First, the oscillator strength of the LPSR band increases with increasing particle size. Second, a narrowing of the LSPR absorption band occurs with increasing particle size in the intrinsic size regime. Third, the maximum of the LSPR absorption band shifts bathochromically with increasing particle size.

Key and lock interaction

Nanocrystals with a concave-shaped region will from now on be called *lock* particles. In addition, nanocrystals with a complementary convex shape will be called *key* particles; see Fig. S8 (ESI†). To investigate the interactions of the colloidal key and lock particles, the particle concentrations of the nanocrystal stock solutions were determined, and approximately, the same particle amounts were mixed with each other in toluene.

Mixing concave manganese oxide lock particles (MONCs) with voids of (9.3 ± 0.9) nm diameter with smaller gold key particles (AuNCs) of (7.5 ± 0.6) nm diameter results in a stable colloidal solution. Even though the keys could geometrically fit into the voids, almost no key-in-lock assemblies can be observed in the TEM micrograph, see Fig. S9 (ESI†). The rare key-in-lock structures could be stochastically overlain particles. The colloidal solution is stable for days without any changes. This experiment is in contradiction with a published work on a gold–iron oxide key–lock system.[1] Up to now, this is the only published experimental work, which outlined the key and lock interaction of colloidal nanocrystals smaller than 15 nm in size. In that regard, George *et al.* synthesized concave iron oxide nanocrystals *via* the cast–mold approach. They used these lock particles in combination with key nanoparticles consisting of gold of two different sizes. Mixing the pure lock and key particle solutions in pure toluene led to the destabilization of the system when the diameter of the keys was smaller than diameter of the void. The AuNCs formed large undefined structures, which were observed *via* dynamic light scattering and TEM. The authors concluded that the AuNCs were destabilized by the void due to the ligands being stripped off while the key dips into the void. The thermodynamic driving force of this process remained unstated.

We have performed several control experiments, which clearly reveal that the findings by George *et al.* are likely not explainable by key–lock interactions but rather by the residual iodine contamination from the etching step of the concave nanocrystals. These experiments are summarized in detail in the ESI (Fig. S10 and S11† and the corresponding discussion).

Many theoretical and also experimental investigations of the key–lock systems at the mesoscale utilized depletion interaction as a thermodynamic driving force to push the keys into the complementary locks.[9–14] Briefly, adding a non-adsorbing polymer to a solution of colloidal hard spheres induces an effective depletion layer on the surface of the particles. The reason for this is the loss of configurational entropy of the polymer in the region near the surface. The respective volume is called excluded volume. If the hard spheres come close enough to each other, the excluded volumes of them will overlap and inherently increase the overall accessible volume for the polymer in the system. This induces an entropic driving force for the system to agglomerate (this means increased accessible volume for the polymer).[21] The depletion interaction is stronger for particles with complementary shapes because in that case the overlap of the excluded volumes is larger. In a system with a mixture of lock and key particles, the entropy of the system will considerably increase if the keys fit into the voids of the locks.

Indeed, adding poly(ethylene glycol) methacrylate (PEGMA) to a mixture of AuNCs and concave MONCs initiates an interaction in the previously stable colloidal solution. The mixture gets turbid after minutes with a PEGMA volume fraction of

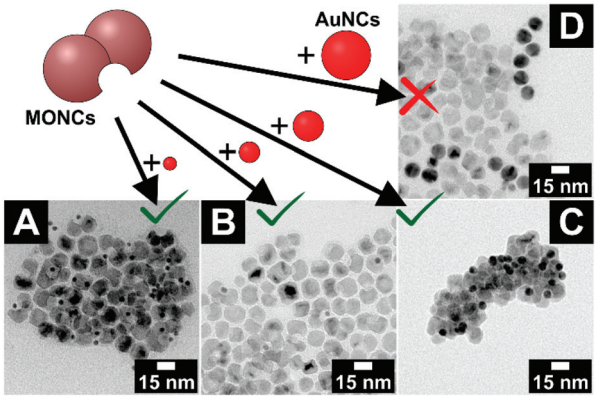

Fig. 4 TEM bright field images of key–lock experiments with quasi-spherical gold nanocrystals (AuNCs) of different sizes and concave manganese oxide nanocrystals (MONCs). While the lock particles with inner void diameters of (9.3 ± 0.9) nm are the same in all experiments, the diameter of the key particles varies from (A) (3.9 ± 0.3) nm to (B) (5.1 ± 0.6) nm, (C) (7.5 ± 0.6) nm and (D) (13.4 ± 0.9) nm. Poly(ethylene glycol) methacrylate was added in a volume fraction of 0.3 to all mixtures to induce depletion attraction.

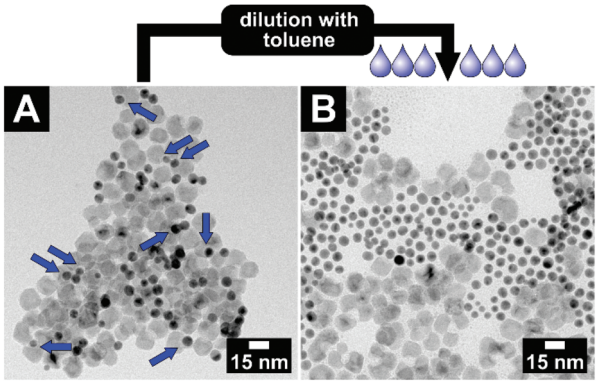

Fig. 5 The reversibility of the key–lock interaction: depletion attraction, the entropic driving force of the system, can easily be reduced or switched off by dilution. TEM bright field images of (A) a key and lock particle mixture with a poly(ethylene glycol) methacrylate volume fraction of φ = 0.3. To guide the eye, the blue arrows point towards key-in-lock assemblies. (B) After dilution of this sample by a factor of roughly 2, no key-in-lock assemblies can be observed anymore.

φ = 0.3. In Fig. 4, the product of four combinations of keys with different sizes and locks with the same void diameter are shown. For the three samples with key particles smaller than the void diameter, key-in-lock assemblies can be seen; see Fig. 4A–C. This proves that depletion interaction takes place and induces not only an agglomeration of the particles but also a specific interaction of the differently shaped particles. In contrast, for the experiment with larger key particles in comparison with the void diameter, no key-in-lock assemblies can be observed at all; see Fig. 4D. (However, if the multiple domains of one concave MONC become somehow fragmented, nanocrystals with a very wide void aperture are formed. These rare particles have such a large concave region that they can also interact with very large gold nanocrystals and key-in-lock combinations can be found; see Fig. S12.†) For geometrical reasons, no key of a larger diameter can enter a smaller void. This means, the void diameter sets an upper threshold for keys that can enter the void. Nevertheless, also this larger-key-smaller-void-solution gets turbid due to agglomeration because the depletion attraction always leads to some kind of unspecific background agglomeration of particles, even in the case of quasi-spherical hard spheres. Especially this unspecific agglomeration of all particles in the samples makes a reliable statistical analysis of the experiments almost impossible, *e.g.* the ratio of the key-in-lock assemblies to separated non-interacted particles. Furthermore, very large agglomerates in the samples could contain different particle amounts of key and lock particles, which would direct the other parts of the system to a non-equilibrium of key and lock particles. Nevertheless, we here clearly report for the first time the depletion attraction driven size-selective recognition of nanoparticles by concave nanoparticles.

This key–lock interaction is a reversible process. All particles of the system are continuously stabilised by a ligand shell and only pushed into assemblies by the pseudo-attractive force of the depletion interaction. If the key–lock system with an initial volume fraction of φ(PEGMA) = 0.3 is diluted with toluene by a factor of roughly 2, the key-in-lock assemblies, as well as all other agglomerates start to dissolve again; see Fig. 5. The product is a stable colloidal solution of key and lock par-

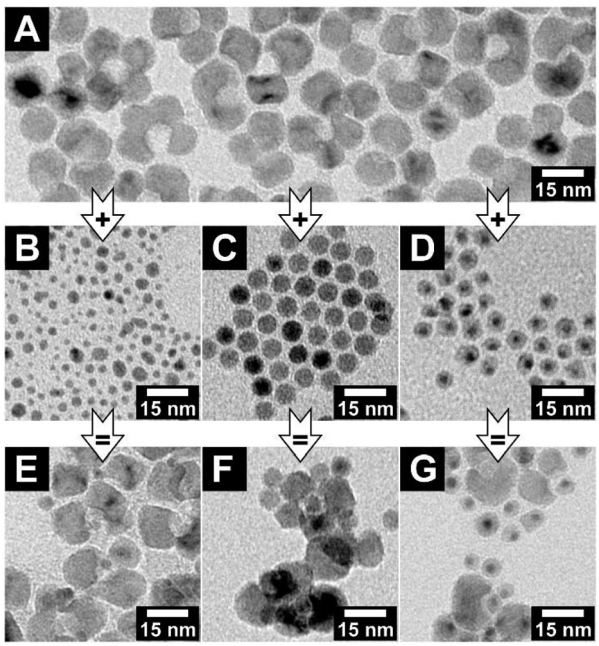

Fig. 6 TEM bright field images of (A) concave manganese oxide nanocrystals with void diameters of (9.3 ± 0.9) nm. (B–D) Pure quasi-spherical silver, iron oxide and gold-nickel sulfide core–shell nanocrystals, with diameters of (3.1 ± 1.2) nm, (7.6 ± 0.4) nm and (6.5 ± 1.0) nm, respectively. (E–G) Key-in-lock assemblies of manganese oxide lock nanocrystals (E) with silver key nanocrystals, (F) with iron oxide key nanocrystals, and (G) with gold-nickel sulfide key nanocrystals.

ticles. The particles are not changed in size and shape in comparison with the pristine key and lock particles.

The interaction of the key and lock particles should exclusively depend on the key and void diameters and not on the kind of material they consist of. To confirm this hypothesis, key particles with appropriate diameters consisting of silver, iron oxide and a core–shell structure of gold-nickel sulfide (and thus particles with very different surface characters) were synthesised. For the structural analysis of the pure nanocrystals, see Fig. S13–S15 (ESI†). In the key–lock experiments, these key particles were mixed with manganese oxide lock particles and the interaction was initiated *via* the addition of PEGMA. For all three material compositions, key-in-lock assemblies can be found; see Fig. 6. The findings for these materials are not as clear as for the gold particles, simply because the well-known and well-established gold particle samples have much narrower size distributions. Nevertheless, they clearly demonstrate that as expected, the depletion attraction driven process at the nanoscale shown in this paper is not a material-related property, but instead only a shape-driven property, which hence should be easily transferrable to other material combinations.

Conclusions

Concave manganese oxide nanocrystals (MONCs), with an accessible void, can interact with convex-shaped nanocrystals of complementary or smaller size and shape. The interaction is analogous to a key–lock system. Only if the convex key particle is smaller than the void of the concave lock particle, the key can enter the void. Additionally, the system requires a driving force to make the nanocrystals interact with each other. Here, depletion attraction was utilized as an entropic driving force, which was enabled by the addition of poly(ethylene glycol) methacrylate to the pristine stable colloidal nanocrystal mixtures. The interaction of key and lock nanocrystals was proven to be dependent on the size but independent of the material composition of the key particles. Quasi-spherical key nanocrystals consisting of gold, silver, iron oxide and gold-nickel sulfide were examined in combination with manganese oxide lock particles. The fundamental experimental findings are the proof of reversible key–lock interaction at the length scale of a few nanometres. This opens up possibilities for the further development of sensory applications to detect nanoparticles with specific sizes utilizing key–lock interactions. In principle, our findings should be extendable towards all types of chemically inert matching key and lock particles, which are mixed with an also chemically inert depletion attraction agent. Further improvements for the quantification of key-in-lock assemblies will have to be done, *e.g.* by the immobilization of lock particles onto macroscopic surfaces like glass slides. Additionally, the shape of the voids will be an interesting parameter for key–lock interactions at the nanoscale. For this purpose, cubic or cylindrical voids can be formed *via* the cast–mold approach using cubic or cylindrical seed particles. Besides the gain of fundamental knowledge, this could open up possibilities for the cheap and fast investigations of nanocrystal shapes without the need for expensive TEM.

Experimental section

Synthetic procedures

Used materials. All starting materials, reagents, and solvents were obtained from commercial vendors and used as received. Acetone (>99.5%), 1-dodecanethiol (98%), hexane (99%), manganese(II) chloride tetrahydrate (>99%), methanol (>99.8%), 1-octadecanethiol (>98%), 1-octadecene (90%), oleylamine (70%), poly(ethylene glycol) methacrylate (M_n = 500), potassium cyanide (98%), silver(I) acetylacetonate (98%), sodium hydroxide (>98%) and toluene (>99.7%) were purchased from Sigma-Aldrich. Iron(0) pentacarbonyl (99.99%) was purchased from Acros Organics. Magnesium sulfate (70%) was purchased from Fisher Chemical. Ethanol (>99.8%) and iodine (99.8%) were purchased from Carl Roth. Borane *tert*-butylamine complex (97%), oleic acid (90%) and 1,2,3,4-tetrahydronaphthalene (97%) were purchased from Alfa Aesar. 18-Crown-6-ether (99%), hydrogen tetrachloroaurate(III) trihydrate (99.99%), nickel(II) chloride hexahydrate (99.9%) and tri-*n*-octylphosphine (97%) were purchased from ABCR.

Synthesis of small gold nanocrystals (d < 6 nm). For the preparation of gold nanocrystals in an up-scaled approach of Peng *et al.*,[22] hydrogen tetrachloroaurate(III) trihydrate (800 mg, 2.0 mmol) was dissolved in a mixture of 1,2,3,4-tetrahydronaphthalene (40 mL) and oleylamine (40 mL) in a 250 mL flask. The precursor solution was cooled to 0 °C. A solution of borane *tert*-butylamine complex (348 mg, 4 mmol) in 1,2,3,4-tetrahydronaphthalene (4 mL) and oleylamine (4 mL) was injected into the gold precursor solution under vigorous stirring. The reaction mixture was stirred for additional 2 h. The product was precipitated by the addition of acetone (≈560 mL), collected by centrifugation (5 min, 5000*g*) and dispersed in toluene. The cleaning procedure was repeated one to two times. Subsequently, the product was dispersed in toluene (40 mL). Increasing the reaction temperature results in smaller nanocrystals. For example, at 40 °C the diameter is roughly 2 to 3 nm.

Synthesis of large gold nanocrystals (d > 6 nm). According to Zhu *et al.*, gold nanocrystals with diameters larger than ≈6 nm were prepared *via* a seed-mediated growth approach with slight variations.[23] For the synthesis of ≈8 nm gold nanocrystals, hydrogen tetrachloroaurate(III) trihydrate (200 mg, 0.5 mmol) was dissolved in a mixture of 1-octadecene (16 mL) and oleylamine (16 mL). Once a clear red-orange solution was obtained, previously prepared gold nanocrystals (30 mg, 5 nm) were added and the solution was heated to 80 °C within 10 min. This reaction temperature was held for additional 2 h. The particles were precipitated by the addition of acetone, collected by centrifugation (5 min, 5000*g*), and dispersed in toluene. For the preparation of ≈13 nm gold nanocrystals, 8 nm gold nanocrystals (10 mg) and hydrogen tetrachloroau-

rate(III) trihydrate (270 mg, 0.675 mmol) were used for a two-step seed-mediated growth approach.

Synthesis of manganese oleate. The synthesis of $Mn(oleate)_2$ was adopted from Schladt and co-workers.[24] Manganese(II) chloride tetrahydrate (7.94 g, 40 mmol) and oleic acid (22.60 g, 80 mmol) were dissolved in methanol (200 mL). Simultaneously, sodium hydroxide (3.2 g, 80 mmol) was dissolved in methanol (200 mL) using an ultrasonic bath. The sodium hydroxide solution was slowly added to the manganese chloride solution under vigorous stirring within roughly 2 h. After completion of the reaction, the waxy solid was washed thoroughly with water, ethanol, and acetone. Afterwards, the product was dissolved in hexane (≈180 mL), dried over magnesium sulfate, filtered, and the solvent was removed under reduced pressure.

Synthesis of gold-manganese oxide hybrid nanocrystals. Gold-manganese oxide hybrid nanocrystals were synthesised according to a previously reported procedure *via* a seed-mediated growth approach with slight variations.[17] First, the ligands of the gold nanocrystals were exchanged. For this ligand exchange, gold nanocrystals (≈10 mg) were added to a solution of 1-octadecanethiol (125 μL) in toluene (1.25 mL) and stirred for at least 2 h under nitrogen. The nanocrystals were precipitated by the addition of methanol (0.5 mL), collected *via* centrifugation (5 min, 3000*g*), and dispersed in toluene. In a three-necked flask, manganese oleate (330 mg, 0.53 mmol) was dissolved in a mixture of 1-octadecene (20 mL), oleic acid (1.9 mL), and oleylamine (2 mL). The pre-treated gold nanocrystals were transferred into the manganese oleate solution and the reaction mixture was degassed at 80 °C for 30 min. Subsequently, the temperature was increased under an argon flow up to 315 °C with 2 °C min^{-1}, held at this temperature for additional 30 min, and subsequently cooled down to 25 °C under argon atmosphere. The nanocrystals were precipitated by the addition of toluene (≈10 mL), acetone (≈20 mL), and ethanol (≈10 mL), collected *via* centrifugation (5 min, 5000*g*), and finally dispersed in toluene (6 mL).

Etching with iodine. In a disposable centrifuge vial (polypropylene), a solution of gold-manganese oxide nanocrystals (3 mL, $\approx 3 \times 10^{-9}$ mol NCs) was mixed with oleylamine (1.5 mL, 4.6 mmol) and oleic acid (1.5 mL, 4.7 mmol). A freshly prepared solution of iodine in toluene (7.5 mL, 3.75 mmol, $c(I_2)$ = 0.5 mol L^{-1}) was added. The reaction mixture was shaken for 40 min. The particles were precipitated by the addition of acetone (≈12 mL) and collected by centrifugation (1 min, 5000*g*). The product was dispersed in toluene (3 mL) and mixed with oleylamine (1.5 mL, 4.6 mmol) and oleic acid (1.5 mL, 4.7 mmol). After the addition of the iodine solution (7.5 mL, 3.75 mmol), the mixture was shaken for 40 min. The whole solution was transferred into a new disposable centrifuge vial (to avoid any residual iodine released from the polypropylene). The particles were precipitated using acetone (≈12 mL) and collected by centrifugation (1 min, 5000*g*). After the liquid phase was discarded, the solid was washed several times with acetone, stored under acetone for 30 min, dried and finally dispersed in toluene (3 mL).

Etching with potassium cyanide. In a disposable centrifuge vial, the gold-manganese oxide hybrid nanocrystal dispersion (0.1 mL, $\approx 1 \times 10^{-10}$ mol NCs) was mixed with oleic acid (0.1 mL, 0.3 mmol) and oleylamine (0.1 mL, 0.3 mmol). If etching should be done in the presence of the phase transfer catalyst, a solution of 18-crown-6-ether in toluene (0.53 mL, β = 100 mg mL^{-1}) was added. Otherwise, pure toluene (0.53 mL) was added. Subsequently, an aqueous solution of potassium cyanide (0.2 mL, c = 1 mol L^{-1}) was added. The reaction mixture was shaken for 10 min, the particles precipitated by the addition of acetone (1 mL) and toluene (≈0.5 mL), collected *via* centrifugation (5 min, 14 100*g*), and dispersed in toluene (0.3 mL).

Synthesis of silver nanocrystals. A suspension of silver(I) acetylacetonate (103 mg, 0.5 mmol) in 1,2,3,4-tetrahydronaphthalene (10 mL) and oleylamine (10 mL) was cooled to 0 °C. A solution of borane *tert*-butylamine complex (88 mg, 1 mmol) in 1,2,3,4-tetrahydronaphthalene (1 mL) and oleylamine (1 mL) was injected under vigorous stirring. After 1 h, the particles were precipitated by the addition of acetone (≈120 mL), collected by centrifugation (2 min, 5000*g*), and dispersed in toluene (≈12 mL) with oleylamine (0.4 mL). The particles were again precipitated by the addition of ethanol (≈40 mL), collected by centrifugation (4 min, 5000*g*), dispersed in toluene, and filtered (syringe filter, 200 μm) to separate the nanocrystals from larger undefined particles.

Synthesis of iron oxide nanocrystals. According to Hufschmid *et al.*, pure iron oxide nanocrystals were synthesised *via* the thermal decomposition of iron(0) pentacarbonyl, but with some variations.[25] In a typical synthesis, oleic acid (0.8 mL, 2.5 mmol) is added to 1-octadecene (10 mL) in a three necked flask. The solution was degassed under vacuum at 100 °C for 30 min. Iron(0) pentacarbonyl (0.2 mL, 1.48 mmol) was added under argon. The reaction mixture was heated to 300 °C within 9 min and kept at the reaction temperature for 30 min. Afterwards, the mixture was cooled down to 25 °C and oxidized under ambient conditions for 15 min. The particles were precipitated by the addition of toluene (10 mL) and acetone (50 mL), collected by centrifugation (5 min, 5000*g*), and dispersed in toluene. The precipitation was repeated by the addition of methanol (30 mL); the particles were collected by centrifugation (5 min, 5000*g*), and dispersed in toluene (4 mL) afterwards. Varying the oleic acid to iron(0) pentacarbonyl ratio will change the diameter of the obtained iron oxide nanocrystals; a higher ratio results in larger diameters.

Synthesis of gold-nickel sulfide nanocrystals. According to a previously reported procedure with some modifications, gold-nickel sulfide hybrid nanocrystals were synthesised *via* a seed-mediated growth approach.[26] In a three necked flask, nickel(II) chloride hexahydrate (6.7 mg, 0.028 mmol) was dissolved in a mixture of 1-octadecene (5 mL) and oleylamine (0.5 mL). The solution was degassed at 80 °C under vacuum for 1 h. Afterwards, the solution was heated to 200 °C under argon atmosphere. A dispersion of gold nanocrystals (4.1×10^{-9} mol NCs) in a mixture of toluene (0.1 mL), 1-octadecene

(0.5 mL), oleylamine (0.25 mL), and tri-*n*-octylphosphine (0.4 mL) was prepared under inert atmosphere and swiftly injected into the hot synthesis solution. Immediately after this injection, a solution of 1-dodecanethiol (65 μL, 0.271 mmol) in 1-octadecene (1 mL) was added dropwise over roughly 1 min. After an additional minute of reaction time, the reaction was stopped by the addition of toluene (5 mL). The product was precipitated by the addition of ethanol (12 mL), collected *via* centrifugation (20 min, 3773*g*), and finally dispersed in toluene (4 mL).

The key–lock interaction *via* depletion attraction. The key–lock experiments were carried out in 500 μL quartz glass cuvettes with 2 mm path length. For a typical experiment with a volume fraction of poly(ethylene glycol) methacrylate of φ(PEGMA) = 0.3, lock nanocrystals and key nanocrystals (each 1×10^{-10} mol NCs) were diluted in toluene with previously added oleylamine (5 μL per 3 mL toluene) to a total volume of 350 μL. Subsequently, poly(ethylene glycol) methacrylate (150 μL, φ = 0.3) was added and the mixture was thoroughly mixed with the help of a syringe. The mixture was occasionally shaken until TEM samples were prepared 30 min after initialisation.

Methods

Electron microscopy. Transmission electron microscopy measurements were carried out using an FEI Tecnai G2 F20 equipped with a field emission gun. The acceleration voltage was set to 200 kV. Samples of pure nanocrystals were prepared by drop casting. The diluted sample was dropped onto a carbon film coated copper grid (300 mesh, Quantifoil), which was previously placed on a filter paper. Also, the key–lock experiment samples were prepared *via* drop casting, but the mixtures were not diluted before dropping onto the TEM grid. To reduce the organic contamination induced by PEGMA, these TEM grids were washed carefully with acetone afterwards.

X-ray diffraction. X-ray diffraction patterns were recorded using a Bruker D8 Advance in Bragg–Brentano-geometry, which was operated at 40 kV and 40 mA. Cu–K_α radiation was used. The samples were prepared by dropping and drying the nanocrystal solution onto a single crystalline silicon holder.

Elemental analysis. The mass concentrations of the nanocrystal stock solutions were determined by atomic absorption spectroscopy. The measurements were carried out at a Varian AA 140 spectrometer. For the preparation of the samples, aliquots were taken, the solvent was evaporated, and the precipitate was subsequently dissolved in freshly prepared aqua regia or nitric acid, diluted with deionized water, and measured against calibration standards with known elemental mass concentrations.

Optical spectroscopy. All optical UV/vis/NIR extinction spectra were recorded using an Agilent Cary 5000 UV/vis/NIR spectrophotometer in transmission mode. Samples of pure nanocrystals were diluted in toluene in quartz glass cuvettes with 10 mm path length. Key–lock solutions were prepared and measured in glass cuvettes with 2 mm path length.

Abbreviations

NCs	Nanocrystals
AuNCs	Gold nanocrystals
MONCs	Manganese oxide nanocrystals
LSPR	Localized surface plasmon resonance
PEGMA	Poly(ethylene glycol) methacrylate
SAED	Selected area electron diffraction
TEM	Transmission electron microscopy
XRD	X-ray diffraction
NIR	Near infra-red

Conflicts of interest

There are no conflicts to declare.

Acknowledgements

D. D. and D. H. acknowledge financial support from DFG Research Grant DO 1580/5-1. R. H. is grateful to the Hannover School for Nanotechnology for financial support. Additionally, the authors would like to thank the Laboratory of Nano and Quantum Engineering for the possibility to use the TEM. The authors wish to thank Armin Feldhoff and Jürgen Caro for providing access to powder XRD measurement facilities.

References

1 C. George, D. Dorfs, G. Bertoni, A. Falqui, A. Genovese, T. Pellegrino, A. Roig, A. Quarta, R. Comparelli, M. L. Curri, R. Cingolani and L. Manna, *J. Am. Chem. Soc.*, 2011, **133**, 2205–2217.
2 S. Kraus-Ophir, J. Witt, G. Wittstock and D. Mandler, *Angew. Chem.*, 2014, **53**, 294–298.
3 H. Wu, Y. Li, D. Kadirov, S. Zhao, X. Lu and H. Liu, *Langmuir*, 2017, **33**, 11817–11824.
4 H. Y. Chang, C. W. Huang, Y. F. Chen, S. Y. Chen, Y. J. Sheng and H. K. Tsao, *Langmuir*, 2015, **31**, 13085–13093.
5 G. van Anders, D. Klotsa, N. K. Ahmed, M. Engel and S. C. Glotzer, *Proc. Natl. Acad. Sci. U. S. A.*, 2014, **111**, E4812–E4821.
6 G. van Anders, N. K. Ahmed, R. Smith, M. Engel and S. C. Glotzer, *ACS Nano*, 2014, **8**, 931–940.
7 Z. Jin and J. Wu, *J. Phys. Chem. B*, 2011, **115**, 1450–1460.
8 P. Y. Wang and T. G. Mason, *J. Am. Chem. Soc.*, 2015, **137**, 15308–15314.
9 U. Okabe, T. Okano and H. Suzuki, *Sens. Actuators, A*, 2017, **254**, 43–53.
10 S. Badaire, C. Cottin-Bizonne and A. D. Stroock, *Langmuir*, 2008, **24**, 11451–11463.
11 T. Tigges and A. Walther, *Angew. Chem.*, 2016, **55**, 11261–11265.

12 S. Sacanna, W. T. Irvine, P. M. Chaikin and D. J. Pine, *Nature*, 2010, **464**, 575–578.
13 S. Sacanna, W. T. M. Irvine, L. Rossi and D. J. Pine, *Soft Matter*, 2011, **7**, 1631–1634.
14 Y. Wang, Y. Wang, X. Zheng, G. R. Yi, S. Sacanna, D. J. Pine and M. Weck, *J. Am. Chem. Soc.*, 2014, **136**, 6866–6869.
15 Y. Wang, Y. Wang, D. R. Breed, V. N. Manoharan, L. Feng, A. D. Hollingsworth, M. Weck and D. J. Pine, *Nature*, 2012, **491**, 51–55.
16 K. J. Bishop, C. E. Wilmer, S. Soh and B. A. Grzybowski, *Small*, 2009, **5**, 1600–1630.
17 I. Schick, S. Lorenz, D. Gehrig, A. M. Schilmann, H. Bauer, M. Panthofer, K. Fischer, D. Strand, F. Laquai and W. Tremel, *J. Am. Chem. Soc.*, 2014, **136**, 2473–2483.
18 J. H. Zubrick, B. I. Dunbar and H. D. Durst, *Tetrahedron Lett.*, 1975, **16**, 71–74.
19 C. J. Pedersen and H. K. Frensdorff, *Angew. Chem.*, 1972, **11**, 16–25.
20 T. Hendel, M. Wuithschick, F. Kettemann, A. Birnbaum, K. Rademann and J. Polte, *Anal. Chem.*, 2014, **86**, 11115–11124.
21 H. N. W. Lekkerkerker and R. Tuinier, *Colloids and the Depletion Interaction*, Springer, 2011, vol. 833.
22 S. Peng, Y. Lee, C. Wang, H. Yin, S. Dai and S. Sun, *Nano Res.*, 2008, **1**, 229–234.
23 W. Zhu, R. Michalsky, O. Metin, H. Lv, S. Guo, C. J. Wright, X. Sun, A. A. Peterson and S. Sun, *J. Am. Chem. Soc.*, 2013, **135**, 16833–16836.
24 T. D. Schladt, T. Graf and W. Tremel, *Chem. Mater.*, 2009, **21**, 3183–3190.
25 R. Hufschmid, H. Arami, R. M. Ferguson, M. Gonzales, E. Teeman, L. N. Brush, N. D. Browning and K. M. Krishnan, *Nanoscale*, 2015, **7**, 11142–11154.
26 R. Himstedt, P. Rusch, D. Hinrichs, T. Kodanek, J. Lauth, S. Kinge, L. D. A. Siebbeles and D. Dorfs, *Chem. Mater.*, 2017, **29**, 7371–7377.